Topographic Enhancement of Tropical Cyclone Precipitation (TCP) in Eastern Mexico

L. Zhu[1], P. G. Aguilera[2]

[1] Department of Geography, Environment, and Tourism, Western Michigan University, Kalamazoo, MI, USA.

[2] Department of Physics, Western Michigan University, Kalamazoo, MI, USA.

Corresponding author: Laiyin Zhu (laiyin.zhu@wmich.edu)

Key Points:

- Topographic enhancement of Tropical Cyclone Precipitation is analyzed based on a 99-year climatology.
- Clustered locations show strong correlation between topographic complexity and Tropical Cyclone precipitation.
- Random Forest models can identify the most important topographic variables and their sensitivities in the Tropical Cyclone Precipitation.

Abstract

Tropical Cyclone Precipitation (TCP) is one of the major triggers of flash flooding and landslide in eastern Mexico. The interactions between the topography of the Sierra Madre Occidental and the TCP of storms from the Gulf of Mexico are still poorly understood. We apply multiple statistical techniques to a 99 year daily TCP record and an elevation data with high spatial resolution. Correlation analysis for the whole dataset is dominated by the strong inland-to-ocean gradient of both TCP and topography. Clusters defined by grids' distances to the coast show significant positive correlations between TCP variables and topographic complexity variables (Range, Standard Deviation, and Slope). The quantile analysis demonstrates that the most extreme TCPs are more likely to locate in grids with higher amounts of topographic complexity (Range and Standard Deviation) than the median and the trivial TCPs. The Random Forest (RF) model is an excellent tool to disentangle complex relationships between TCP and topography. The models show that the grid's location and aspect of the slope aspect are the two most important variables that affect the TCP statistics. TCP in eastern Mexico is sensitive within two zones: (1) Low lying coastal regions with lower elevation and less topographic complexity. (2) The mountainous region with higher elevation and topographic complexity, especially with the slope facing the windward direction to the Gulf. All results support that the topography in eastern Mexico has an enhancing effect on the TCP.

1 Introduction

Tropical Cyclone Precipitation (TCP) is one of the major triggers of flooding and landside over the land. Various studies (Emanuel, 2017; Knutson et al., 2019; Risser & Wehner, 2017; Trenberth et al., 2018) have argued that anthropogenic global warming may increase the chance of extreme TCP events like Hurricane Harvey in 2017. Some have attributed those increases to energy support from the heated oceans (Trenberth et al., 2018). For those Tropical Cyclones (TCs) that made landfall, the surface-atmosphere interaction is quite different from that when they are over the oceans. The TCP processes over land can be quite complex and are influence by many factors, including the moisture and energy that the storm brought from the ocean, the size, translation speed, and intensity of the storm, surface conditions of the land (moisture and energy), land use and cover, interactions with other weather systems, and the topographic features (Arndt et al., 2009; Kimball, 2008; Tuleya, 1994; Zhang et al., 2018).

Although the influence of topographic features on different kinds of precipitation systems have been extensively discussed by different pieces of literature, Houze (2010) reviewed orographic effects on all types of precipitation systems and concluded that the mechanism of how TCP is affected by mountains is understudied. Research on this topic can be categorized as theoretical modeling, observational data analysis, and numerical modeling of storm cases. Early numerical simulations indicate that the topographic features not only alter the structure and energy inside of the storm but also affect the basic flow that steers the TCs (Bender et al., 1985, 1987). Most current theoretical TCP models (Langousis & Veneziano, 2009; Lu et al., 2018) are based on the calculation of water vapor flux of the low-level convergence of horizontal wind. One very important parameter in those theoretical TCP models is the surface drag coefficient, which describes the surface roughness that influences the low-level convergence and the TCP intensity (Kepert, 2001; Langousis & Veneziano, 2009; Shapiro, 1983). However, the current theoretical parametric TCP model usually does not consider the influence of topography on the surface roughness, which can significantly alter the rainfall pattern.

Advances in remote sensing helped the understanding of interactions between TCs and topography in much more details. Radar has been used to observe the wind and rain field in landfalling TCs with strong interactions with the orography. Wind profiler radar shows that the wind has been deflected with a strength that may cause a secondary circulation or block the previous storm circulation system in two typhoons that interacted with the Central Mountain Range (CMR) of the Taiwan Island (Pan et al., 2008). Yu and Cheng (2008) used Doppler radars to observe Orographic enhanced precipitation in Typhoon Xangsane in 2000. They discovered that background storm precipitation and profile of the mountains are both important to the enhancement with larger precipitation observed over the narrower and lower barrier. R. B. Smith et al. (2009) used multiple sources of observation from remote sensing and gauges as well as a linear model to study the enhancement of the precipitation in Hurricane Dean in Dominica. They conclude that the enhanced precipitation is not likely from the new convection triggered by the land but more possible to be due to the seeder-feeder mechanism. This mechanism is happening at a faster speed than the inland convections with falling raindrops of TCs gathering cloud-water sourced from the complex terrains (Bergeron, 1968; Ronald B. Smith, 1979).

Various simulations based on dynamic weather models also demonstrated the mechanism of how topography enhances TCP. Wu et al. (2002) used a Mesoscale Model (Penn-State MM5) to simulate rainfall from the Typhoon Herb and discovered that a significant forced lifting of airflow associated with the interaction between the storm's circulation and the CMR of the Taiwan island. Similarly, Lin et al. (2002) proved that the topography is a major forcing of rainfall in the mountains of Taiwan than the original rain bands. Li et al. (2007) demonstrated that the condensational heating is an important process in the southeastern China terrains and drastically increased the precipitation in Typhoon Aere in 2004 by using a Regional Eta-coordinate Model. Severe TC Larry in Australia was also simulated in both no topography and topography scenarios (Ramsay & Leslie, 2008). Localized maximum precipitation exists in elevated regions in the simulation with topography. And precipitation in the simulation without topography is more symmetric. More recently, Huang et al. (2020) used an idealized Weather Research and Forecasting (WRF) model to test the sensitivity of TCP to vortex core size, intensity, and steering wind speed for TCs passing CMR in Taiwan. They concluded that the influence between topography and TCP is a complex interaction of vortex track, landfall position, and the structure of the vortex circulation. The mountain range in Taiwan can deflect or even block the westward-moving TC systems in the pacific (Lin et al., 2005). Houze (2012) provided a physical mechanism for the lifting effect of tropical cyclones by the orography. While TCs are over the ocean they tend to be moist neutral and the uniform warm ocean boundary makes the flow slightly unstable. The lifting over the mountainside release this instability and trigger the convective cells on the windward side and then interact with the gravity wave on the lee side of the mountain.

Mexico is a country prone to attacks of TCs on both sides of coasts facing the Pacific Ocean and the Gulf of Mexico. TCP can contribute 0 to 40% of the annual precipitation across Mexico, which is estimated from the satellite precipitation product TMPA 3B42 from 1998 to 2013 (Agustín Breña-Naranjo et al., 2015). Franco-Díaz et al. (2019) used the same product and estimated that TCs contribute 10 to 30% of total precipitation from July to October and are associated with 40 to 60% of daily extreme rainfall (> 95th percentile) in the coastal area. Extreme TCP events are triggers of severe flooding with massive disruption to the society and intense economic losses (Agustín Breña-Naranjo et al., 2015). One example is the incident of two TCs (Tropical Storm Manuel in the Pacific and Hurricane Ingrid in the Gulf of Mexico) stroke Mexico between September 13 and 20 in 2013. Flooding from extreme precipitation has damaged 45000 homes with $900 million of insured losses and $5.7 billion in total economic losses. Mexico is a mountainous country with complex topography. Some existing studies have looked at the influence of orography to precipitation system like North American Monsoon (Vivoni et al., 2007), and general precipitation in Mexico (Mascaro et al., 2014; Pineda-Martinez & Carbajal, 2009). Several theoretical and case studies (Farfán & Cortez, 2005; Farfán & Zehnder, 2001; Zehnder, 1993) have been focused on the orographic effect on TCs on the Pacific coast of Mexico, from the Sierra Madre mountains. There is a lack of study that is focused on how orography influences the precipitation of landfall TCs from the Gulf of Mexico on the eastern coast of Mexico. Our approach is different from most of the previous studies for this topic, which are mostly based on single or several cases of TCs. We will systematically look at this topic by using a 99-year daily gridded record of TCP derived from a large number of rain gauges. It is possibly the longest climatological record we can find for the TCP with acceptable spatial details. Topographic characteristics are calculated for each 0.25° grid box from the Digital Elevation Model (DEM) with a high spatial resolution (1 km). The relationships between TCP and different topographic characteristics will be analyzed. We will not only focus on only the general TCP but also the most extreme TCP and it's probability. We will use several statistical techniques to explore the relationships in the data: including traditional techniques of the correlation analysis, k-means clusters, and quantile comparison, as well as the new non-parametric machine learning model Random Forest.

The article is organized as follows. Section 2 will introduce the data and methods of analysis with more details. In Section 3, we will present the results with three focuses. The first will be the general statistical analysis including the correlations and quantile comparisons based on the whole dataset. The second will be on the Random Forest modeling of TCP variables based on locational and topographic variables. We will also develop models only using topography variables to explain their influences independently. The third focus will be on the most intense TCP cases in Mexico's 99-year history of climatology. We will compare the topography of the locations for those most extreme cases with that for locations for those median TCPs and see whether there are systematic differences. We will summarize and discuss our findings in Section 4.

2 Data and Methods

2.1. Precipitation

The TCP is extracted from two major pieces of information: daily rain gauges and locations of the TCs. We have already updated the collection of daily rain gauge observations for both the U.S. and Mexico from 1920 to 2018 from two sources in another study (Zhu & Quiring, 2017). The Daily Global Historical Climatology Network (GHCN-D) covers both the U.S and Mexico with 35161 gauges. The density of gauges is good for the spatial interpolation to even grids at 0.25° in the U.S, but not dense enough for Mexico. Therefore, we collect a second source of daily gauge precipitation for Mexico from the National Weather Service of Mexico, which contains a total of 2526 gauges. Daily TCP is collected from rain gauges within the daily TC boundary, which is defined by connected moving circles with a radius of 800 km. The center locations of those circles are defined by the storm center locations with a 6-hour interval provided by the International Best Track Archive for Climate Stewardship (IBTrACS). We correct the possible wind introduced under-catch in the rain gauge and optimize the Inverse Distance Weighting (IDW) parameters for the spatial interpolation. Those are finished by comparing our gridded TCP data with the Tropical Rainfall Measuring Mission (TRMM) Multi-satellite Precipitation Analysis (TMPA) product 3B42 (Zhu & Quiring, 2017). The final daily TCP grids with 0.25° spatial resolution are clipped by daily boundaries defined by the connected

500 km radius. We use 800 km circles for the step of TCP gauge collection to avoid bias on the edges of 500 km circles when we are doing the IDW spatial interpolation. It yields 4373 TCP days for the whole North American Continent. If we only look at TCP received by Mexico locations, there are 1442 TCP days between 1920 and 2018. The daily TCPs are also aggeregated into storm total accumulated TCP, which yield 399 TCP events in the same time span. In the detailed analysis in the Section 3, we also calculate percentile precipitations (e.g., 95 Percentile or P95) and probabilities that exceed certain percentile TCP for different TCP samples for comparison purposes.

2.2. Topography and Location

We obtain the raw elevation data from the Global 30 Arc-Second Elevation (GTOPO30) offered by the Earth Resources Observation and Science (EROS) Center of the United States Geological Survey. The GTOPO30 has a 1 km resolution and was derived from a variety of sources, which was finished in 1996. We first use the shapefile of Mexico's boundary to subset the whole data in ArcGIS by the Environmental Systems Research Institute (ESRI). Then the statistics of elevations are calculated for each precipitation grid box (0.25°X0.25°) that contains ~ 750 elevation points. We calculate seven variables from the GTOPO30 elevation data to describe the topographic feature of each 0.25° grid. Basic elevation statistics include the mean, maximum, minimum, range, and standard deviations of the elevation sample in each box. All those elevation statistics have the unit of meter. The slope and its' aspect are calculated by the algorithm (Burrough et al., 2015) provided by the ESRI ArcGIS zonal statistics package. The slope describes the ratio between the rise and the run (tan θ) and the aspect describes a slope's major orientation angle from the normal (north as 0°). We also calculate the sphere distance from each 0.25° grid to the nearest coastline of the Gulf of Mexico since there is normally a decaying of TCP from coast to inland.

2.3. Statistical Methods

To explore the relationships between TCP variables and the topographic and location variables, we apply the pairwise correlations (Spearman's ρ) and report all p-values (<0.01 and <0.05) (Best & Roberts, 1975). Because of the strong coast to inland gradient in the TCP, we used the K-means clustering technique to group all grids into six categories based on their distances to the Gulf coast. Analysis within K-means groups can reveal more distinctive relationships between TCP and topography. We also apply percentile analysis for samples of the TCP data from both the whole dataset and the extreme case studies. For example, we find the locations with TCP that are larger than the 99.9 Percentile ($P_{99.9}$, the most extreme cases of the TC.P) as well as the locations with TCP that are between 49.95 and 50.05 Percentile ($P_{49.95}$ and $P_{50.05}$, the cases with the median amount of TCP). We then compare the two groups of locations' topographic features and find whether there are some significant differences between the sample medians by using the Mann-Whitney U-test (Mann & Whitney, 1947).

Both the correlation and the quantile analysis can provide us some insights into how topography features influenced TCP quantitatively. However, those traditional statistical techniques have the shortcomings of normally focusing on one topographic variable for each comparison and can't deal with the combined effects from multiple topographic variables to TCP. It is also very challenging to explain variables with special distributions like latitude and longitude or slope aspect with a cyclic change from 0 to 360°. The Random Forest (RF) Model is a powerful machine learning technique that is based on ensembles of decision trees (Breiman, 2001; Breiman et al., 1984). It has a much less stringent requirement for distribution or type of independent variable. Since the orographic influence on TCP is a complex process with multiple factors working together, and some of our explanatory variables are not normally distributed, we believe the RF model is the best candidate to explore the relationships between topographic variables and TCP extracted from many storms in a long term climatology. The RF models can also rank the importance of individual variables in the model and reveal relationships and sensitivities between independent variables and response variables (Greenwell, 2017).

3 Results, or a descriptive heading about the results

3.1. Spatial Distribution

Seven different topographic characteristics are calculated for each 0.25° grid box from the 1km resolution DEM. They are Mean, Max, and Minimum elevations, elevation Range and Standard Deviations, Slope, and Slope Aspect. Figure 1 shows the map for four major topographic features. We can observe that Mexico has mountainous areas with > 3000 meters

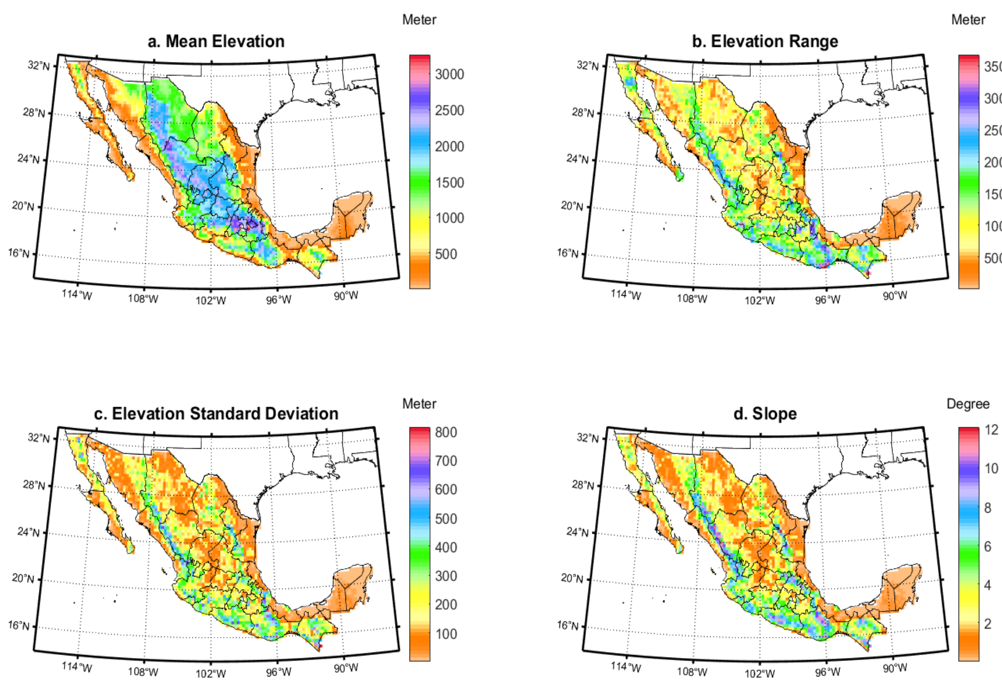

Figure 1. Elevation characteristics in Mexico calculated for 0.25° grids.

Mean elevation in the central and > 500 meters elevations on the coast (1a). The elevation Range (1b), Standard Deviation (1c), and Slope (1d) are demonstrating more complex spatial variations and they share some similarities. Particularly, on the windward side of the Gulf of Mexico, all three topographic variables are demonstrating abrupt changes from the coastal to more inland areas, which might lead to uplifts or seed-feeder effect of the cloud and strengthen convective precipitation like TCP.

TCP can be characterized in many ways. Based on the available spatial and temporal resolution of the data, we define five TCP variables for the analysis. The Annual Mean TCP (AMTCP) is calculated by dividing all aggregated daily TCP by 99 years at each grid. The Maximum Daily TCP (MaxDTCP) is calculated by picking the highest daily TCP from 99 years for each grid. The Maximum Event TCP (MaxETCP) identifies the 99 year maximum of the event total TCP. Then we calculate the 95 percentile (P_{95}) thresholds of both daily and event TCPs for entire Mexico in 99 years. The Probability that TCP exceeds the P_{95} value is calculated as the times the P_{95} value has been exceeded divided by 99 years. We calculate it for all grids for both the daily TCP dataset (DTCPGP95 for Daily TCP Greater than P_{95}) and the event dataset (ETCPGP95 for Event TCP Greater than P_{95}). Figure 2 displays the spatial distributions of AMTCP, MaxDTCP, MaxETCP, and ETCPGP95. The AMTCP is showing a decreasing pattern from the coast to inland, with some high values in the central east Mexico and the neck of the Yucatan Peninsula. The decreasing gradient from the coast to the inland is not as strong as the AMTCP for the MaxDTCP, MaxETCP, and ETCPGP95. Some inland locations are showing the maximum values. There are local maximums clustered in central-east Mexico for the MaxETCP and ETCPGP95.

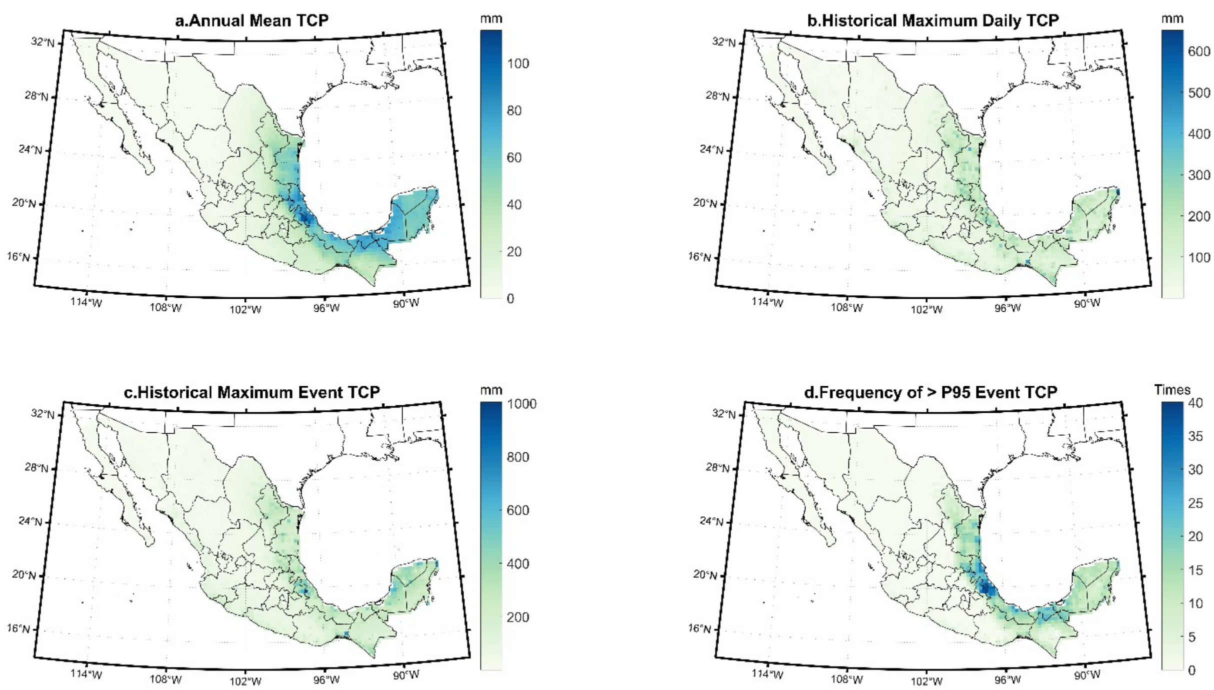

Figure 2. Four TCP variables for Mexico based on a 99 year climatology.

3.2. Correlation and Quantile Analysis

The correlations for pairs of topographic variables and TCP variables are shown in Table 1. Since the TCP is very sensitive to the distance from the location to the coastal line, we calculated the distance from every grid to the nearest coastal line that is facing the Gulf of Mexico (the "Distance" variable in Table 1). The Distance demonstrates the strongest negative

Table 1. Correlation between TCP variables and Environmental Variables for all Grids.

Variables	Mean	Max	Min	Range	Std	Slope	Aspect	Distance
AMTCP	-0.39**	-0.38**	-0.38**	-0.18**	-0.15**	-0.17**	-0.24**	-0.74**
MaxDTCP	-0.39**	-0.34**	-0.40**	-0.09**	-0.06**	-0.07**	-0.22**	-0.66**
MaxETCP	-0.41**	-0.38**	-0.41**	-0.13**	-0.11**	-0.11**	-0.22**	-0.68**
DTCPGP95	-0.44**	-0.38**	-0.42**	-0.18**	-0.12**	-0.11**	-0.24**	-0.59**
ETCPGP95	-0.44**	-0.41**	-0.43**	-0.16**	-0.14**	-0.18**	-0.23**	-0.59**

** indicates p<0.01, * indicates p<0.01, Distance is for Distance from each grid to the nearest coastal line of Gulf of Mexico.

correlations to all TCP variables indicating the strong gradient of TCP from the coast to inland. All other topographic variables are showing statistically significant negative correlations with the TCP variables. We believe that those negative relationships are strongly influenced by the Distance variable because the elevation generally rises with more complexity as we move from the coast to the inland in eastern Mexico. We are not able to find any signal for the topographic enhancement of TCP by simply correlating the two because they are contrarily determined by the location.

To further demonstrate the relationship between topography and the TCP, we must compare them within a region of grids with a similar distance to the coastal line. Therefore, we used the Distance as the criteria for a K-Means clustering, which divides the whole set of grids into six clusters according to each grid's distance to the nearest coastal line (Figure 3). We are

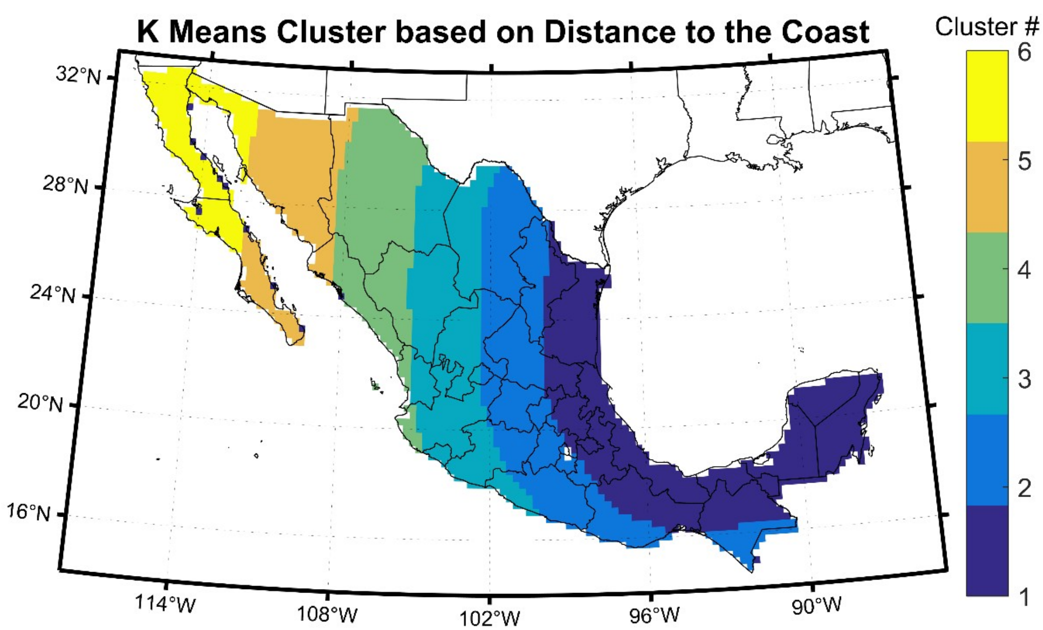

Figure 3. K-Means Clusters of grids calculated based on their distances to the nearest coastal line that is facing the Gulf of Mexico.

only focusing on Cluster 1 and 2 here since they are where most of TCP from Atlantic TCs are located in Mexico (Figure 1). The Cluster 1 and Cluster 2 grids are within 93.50 and 340.18 km to the coastal line, respectively. We calculated the paired correlations between topographic variables and TCP variables for both clusters. The correlation coefficients in Table 2 and 3 are

Table 2. Correlation between TCP variables and Elevation variables for grids in cluster #1 (Coastal Grids).

Variables	Mean	Max	Min	Range	Std	Slope	Aspect
AMTCP	-0.30**	-0.14*	-0.32**	0.21**	0.18**	0.23**	0.24**
MaxDTCP	-0.43**	-0.17**	-0.47**	0.30**	0.24**	0.36**	0.21**
MaxETCP	-0.58**	-0.21**	-0.65**	0.44**	0.34**	0.48**	0.25**
DTCPGP95	-0.46**	-0.25**	-0.49**	0.25**	0.22**	0.36**	0.18**
ETCPGP95	-0.50**	-0.34**	-0.50**	0.18**	0.14*	0.35**	0.18**

** indicates p value<0.01, * indicates p value<0.05

Table 3. Correlation between TCP variables and topographic variables for grids in cluster #2 (Inland Grids near Coast).

Variables	Mean	Max	Min	Range	Std	Slope	Aspect
AMTCP	-0.28**	-0.05	-0.35**	0.36**	0.29**	0.36**	0.03
MaxDTCP	-0.48**	-0.24**	-0.50**	0.31**	0.23**	0.39**	-0.02
MaxETCP	-0.50**	-0.22**	-0.54**	0.39**	0.31**	0.42**	-0.03
DTCPGP95	-0.49**	-0.23**	-0.51**	0.33**	0.24**	0.37**	0.01
ETCPGP95	-0.37**	-0.13*	-0.38**	0.31**	0.21*	0.32**	0.02

** indicates p value<0.01, * indicates p value<0.05

showing a very different pattern than Table 1. Only the Mean, Max and Min elevations have a negative correlation with TCP variables. The dominating impacts from the distance to the coast have been largely removed. The Range, Standard Deviation, and Slope are all demonstrating statistically significant positive correlations with the TCP variables. It indicates that the TCP is enhanced at the locations where elevation is changing fast. Particularly, in cluster 2, where the topography is more complex than cluster 1, the positive correlations are showing more stable with higher average values than Cluster 1. The MaxETCP has the highest mean correlations with the Range, Standard Deviation of the Elevation and the Slope for both Clusters 1 and 2. It indicates that regions with abrupt changes in elevation have stronger enhancing effect for TCP.

The most extreme TCP events are the most important parts of the whole dataset because they can generate a massive amount of rain-water into mountain ranges and watersheds and introduce a higher risk of flash flooding and landslide. Here we select the most extreme TCPs (precipitation > $P_{99.9}$), the median TCPs (precipitation between $P_{49.95}$ and $P_{50.05}$) and trivial TCPs (precipitation < $P_{0.01}$) and compare the topographic variables for their locations. We want to show how topographic characteristics differ between the most extreme precipitation locations and the median and trivial ones. We pick the Elevation Range and Standard Deviation for the comparison because they both show high positive correlations with TCP variables. The comparisons are repeated for the whole data, cluster 1, and cluster 2. Large differences between the most extreme TCP ($P_{99.9)}$ and median TCP ($P_{50)}$ can reach 167.62 mm for daily comparison and 337.05 mm for Event comparison. Box plots (Figure 4a and 4b) and Man-Whitney U-test (Table 4 and Supplement 1) show that the most extreme daily TCP locations have significantly

Table 4. Comparison of quantile TCPs and their associated elevation Range

	Daily TCP						Event TCP					
Category	$P_{99.9}$ TCP	Elev Range	P_{50} TCP	Elev Range	$P_{0.1}$ TCP	Elev Range	$P_{99.9}$ TCP	Elev Range	P_{50} TCP	Elev Range	$P_{0.1}$ TCP	Elev Range
Whole	**164.15**	**767**	7.99	654^{+}	0.01	152^{+}	**318.09**	**276**	15.30	861	0.04	638
Cluster 1	**176.50**	**687**	8.88	138^{+}	0.01	130^{+}	**357.48**	**205**	20.43	255	0.03	195
Cluster 2	**122.49**	**2074**	7.38	983^{+}	0.04	1106^{+}	**220.49**	**1818**	13.20	1013^{+}	0.07	1025^{+}

"+" indicates the current elevation Range sample median is smaller than the elevation Range sample for the $P_{99.9}$ TCP in the same category, using the Mann-Whitney U-test at the 5% significance level. TCP has a unit of mm and Elevation Range has a unit of meter.

larger elevation range and standard deviation than the median TCP and trivial TCP locations. It indicates that the most extreme daily TCPs tend to happen more frequently at locations with more complex topography. Those patterns are weaker for the event TCP (Figure 4c and 4d). No

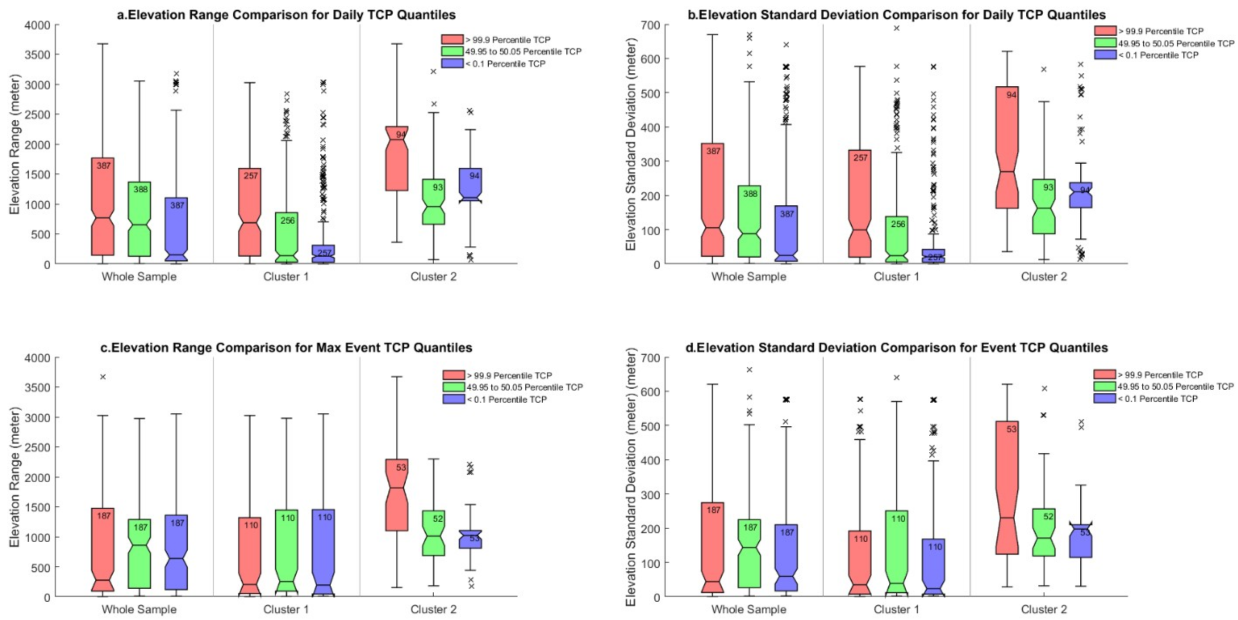

Figure 4. Comparison for Elevation Range and Standard Deviation between the most extreme TCPs ($>P_{99.9}$), median TCPs (between $P_{49.95}$ and $P_{50.05}$), and trivial TCPs ($<P_{0.1}$)

distinct difference in elevation ranges and standard deviations are observed for the comparison for the whole sample and Cluster 1 grids. Only Cluster 2 demonstrates a significantly higher elevation range and standard deviation for the extreme TCP locations than those for other TCP locations (Table 4 and Supplement 1). Cluster 2 grids are located more inland than Cluster 1 grids with a more complex topography and less probability of extreme TCPs. But those extreme TCP cases are more sensitive to the topography changes.

3.3. Random Forest Modeling

RF models are developed for all five TCP variables using locations and topographic information as independent variables to understand they influence TCP collectively and their importance. We develop two models for each TCP variable, the Total models have the complete 10 independent variables including both location and topographic characteristics; the

Topographic (Topo) models only contain 7 topographic features. We want to understand the most important variables for TCP globally as well as the most important topographic variables.

Table 5 is showing statistics for the 3 Total Models and 3 Topo Models we have chosen to represent all 10 models. Statistics for the other 2 total and 2 topo models are shown in Supplement 2. All Total Models demonstrate a very high amount of explained variance (>85%),

Table 5. Information about Random Forest Models developed for three TCP variables: AMTCP, MAXETCP and ETCPGP95. The importance is calculated as the percentage of increased MSE (%IncMSE) if the variable is removed

	AMTCP Total Model		AMTCP Topo Model		MaxETCP Total Model		MaxETCP Topo Model		ETCPGP95 Total Model		ETCPGP95 Topo Model	
Variance Explained	96.66%		59.18%		86.09%		51.25%		90.91%		54.15%	
Importance Rank	Var Name	%Inc MSE	Var Name	%Inc MSE	Var Name	%Inc MSE	Var Name	%Inc MSE	Var Name	%Inc MSE	Var Name	%Inc MSE
1	Dist	38.99	Asp	69.57	Lat	42.55	Asp	49.59	Dist	41.31	Asp	64.64
2	Lon	36.69	Slope	56.39	Lon	37.56	Range	32.68	Lat	38.96	Slope	41.19
3	Lat	30.00	Range	37.90	Dist	29.15	Std	32.22	Lon	27.82	Range	30.30
4	Min	19.18	Max	34.81	Range	20.33	Slope	29.79	Min	20.95	Std	28.18
5	Slope	16.58	Std	32.82	Slope	16.65	Max	25.80	Max	18.04	Mean	22.84
6	Max	15.05	Min	29.27	Std	16.64	Mean	16.60	Mean	17.18	Max	21.98
7	Mean	14.07	Mean	27.38	Max	15.7	Min	11.83	Std	16.85	Min	21.89
8	Asp	11.71			Min	14.91			Asp	16.18		
9	Range	11.28			Asp	14.26			Slope	15.76		
10	Std	10.80			Mean	11.9			Range	15.32		

which is caused by the more complete information in their independent variables. The Distance, Longitudes, and Latitudes are the three most important variables in all Total Models. Longitudes and Latitudes control the relative position between each grid to storm tracks. The proximity to the storm will determine how much precipitation each grid will receive. The distance has a high importance rank in Total models. We have already shown a very strong negative relationship between the Distance and TCP in the previous section. The minimum elevation has the highest importance rank among all topographic variables. Variables that describe the topographic complexity, such as the elevation Range and Slope, are showing high importance rank in some Total models (MaxETCP).

The partial dependence plot describes the marginal effect (sensitivity) from individual independent variables to the dependent variable (Breiman, 2001) in RF models. It shows that the sensitivity of AMTCP drops as the Distance increases or the longitude becomes more toward the west (Figure 5a and b). It generally matches the spatial distributions of the TCP. The lower

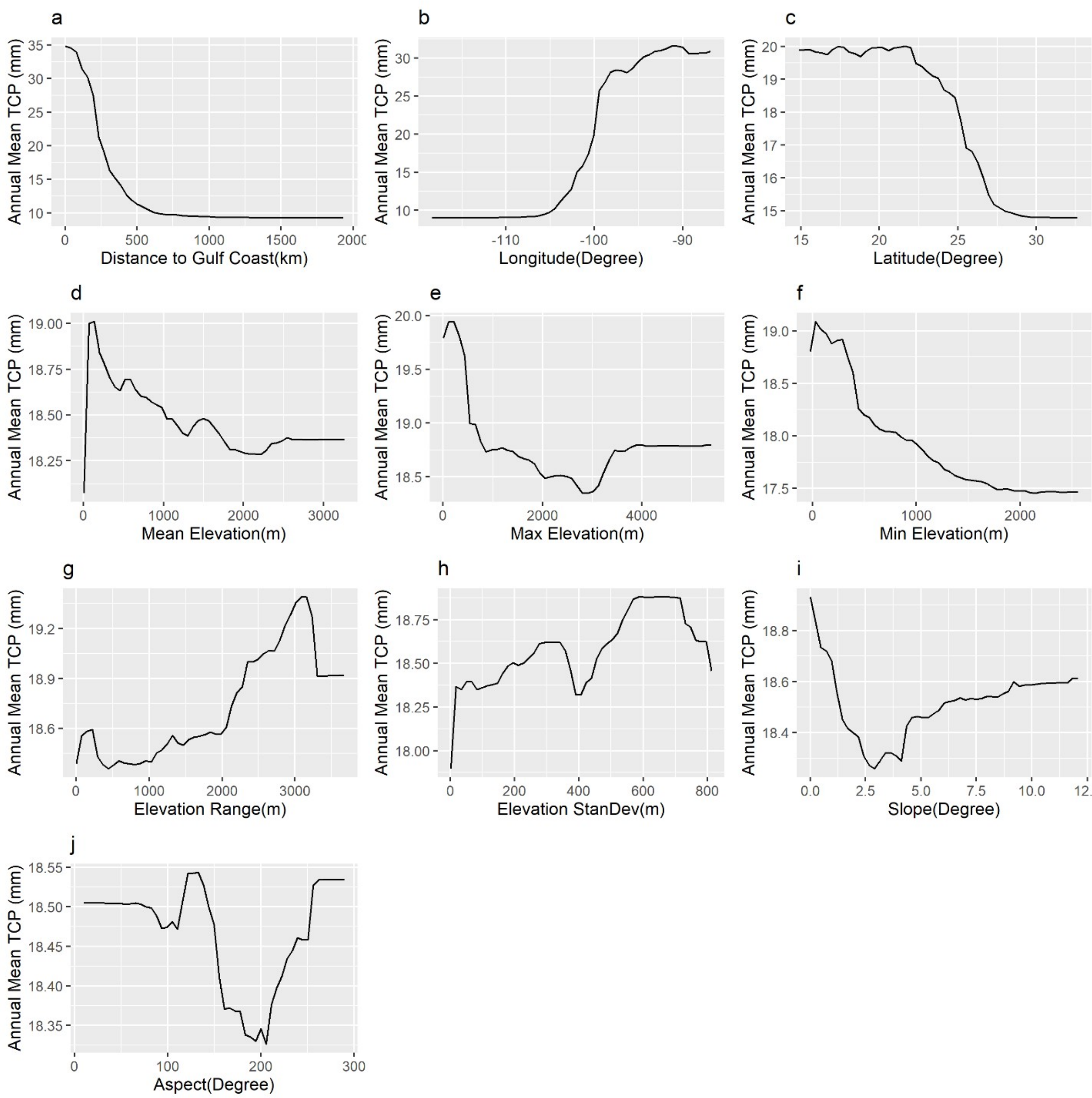

Figure 5. Partial Dependence Plot for variables in the total RF model for the Annual Mean TCP.

latitude observes higher sensitivity of TCP values (Figure 5c), which is due to that lower latitude normally observes higher frequency of TC tracks. There is a general decreasing TCP sensitivity when elevations are increasing (Figure 5d, e, f). However, unlike the monotonous change in plots for location variables, the Mean and Max elevation show more non-linear TCP sensitivity changes. Particularly, we can observe suddenly rise of TCP sensitivity when the mean elevation is at 500 meters and 1500 meters (Figure 5g). There is also an elevated TCP sensitivity plateau when the maximum elevation is greater than 3000 meters. This is an interesting pattern and might be related to the topographic enhancement of TCP by mountains. Figure 6 demonstrates the TCP sensitivity responses to selected couples of independent variables for the Total model of AMTCP. There is a strong influence of TCP sensitivity from the Distance. The highest sensitivity of TCP is located within 200 km of the coastal line and between 50 to 1200 m in mean elevation (6a).

Higher values of elevation Range and Standard Deviation generally lead to higher TCP sensitivity (Figure 5g and 5h). The TCP becomes more sensitive when the elevation Range is larger than 2000 m and the elevation Standard Deviation is between 400 and 800 meters. The TCP sensitivity is high at a very shallow Slope, drops sharply and reach to the lowest at slope value of 2.5°, and increases with steeper slope values (Figure 5i). Coastal areas have very shallow steep slopes but high spatial variabilities in TCP, the cloud lifting effect increases gradually when it moves to more inland with steeper slopes. This pattern is also shown in Figure 6b, where the highest TCP sensitivity is demonstrated in a region with very low mean elevation and shallow slope. But the TCP sensitivity increases again when the Slope becomes steeper (> 5°). Finally, the slope Aspect is demonstrating an interesting pattern for the TCP sensitivity in Figure 5j. When the slope is facing the Gulf of Mexico (with aspect between 0 to 180), there is a much higher TCP sensitivity. Particularly, the TCP sensitivity peaks at the aspect angle of 120°. This is an angle that is vertically intersected with the mean translation direction of landfalling Atlantic TCs if we consider the β effect of the TC motion in the northern hemisphere (Chan, 2005). But when the slope is facing the lee side (with aspect between 180° to 360°), particularly between 150° to 250°, the TCP is much less sensitive to the slope with the minimum reached when the Aspect is ~ 200°. When the Aspect is greater than 250°, the sensitivity increases again, which might be caused by those occasionally stalled TCs moving from the north to south. This pattern can also be observed in Figure 6c. Particularly, we can observe a stripe of enhanced TCP sensitivity when the Aspect is between 110° to 150°, it is even strengthened when the Slope is steeper (> 5°). Figure 6c also shows the dipole of high TCP sensitivity for both shallow and steep regions of the Slope (< 1° or > 5°).

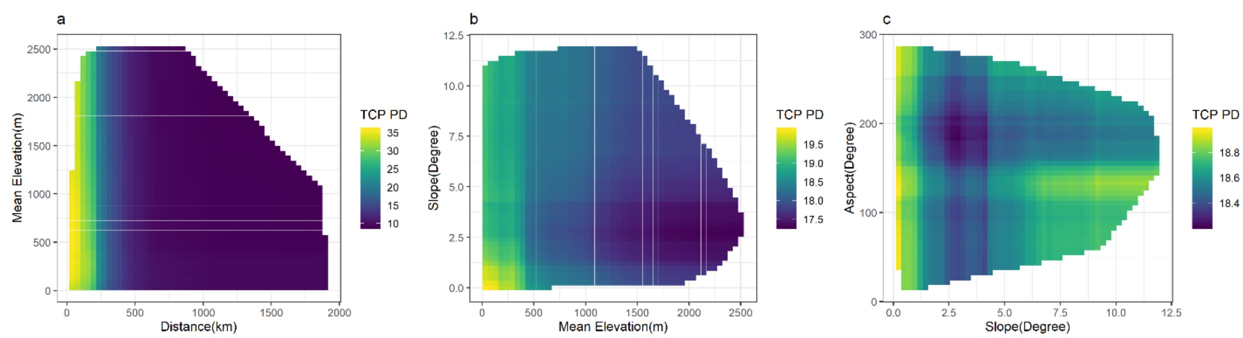

Figure 6. Selected Partial Dependence (PD) Plots for coupled variables in the Total RF model for the Annual Mean TCP.

The Topo models also show high explained variance (>50% on average), there are some changes in the variable importance rankings (Table 5, Supplement 2). The Aspect ranks as the most important variable in all the topographic models. The topography complexity variables (Slope, Standard Deviation, and Range) rank higher than other topographic variables including the Mean, Max and Minimum. The patterns of TCP marginal changes in partial dependence plots are similar to those for total models and show the same directions of changes (Figure 7, Supplement 3, 5, 8, 10). Here we are demonstrating the plot for the MaxETCP as an example.

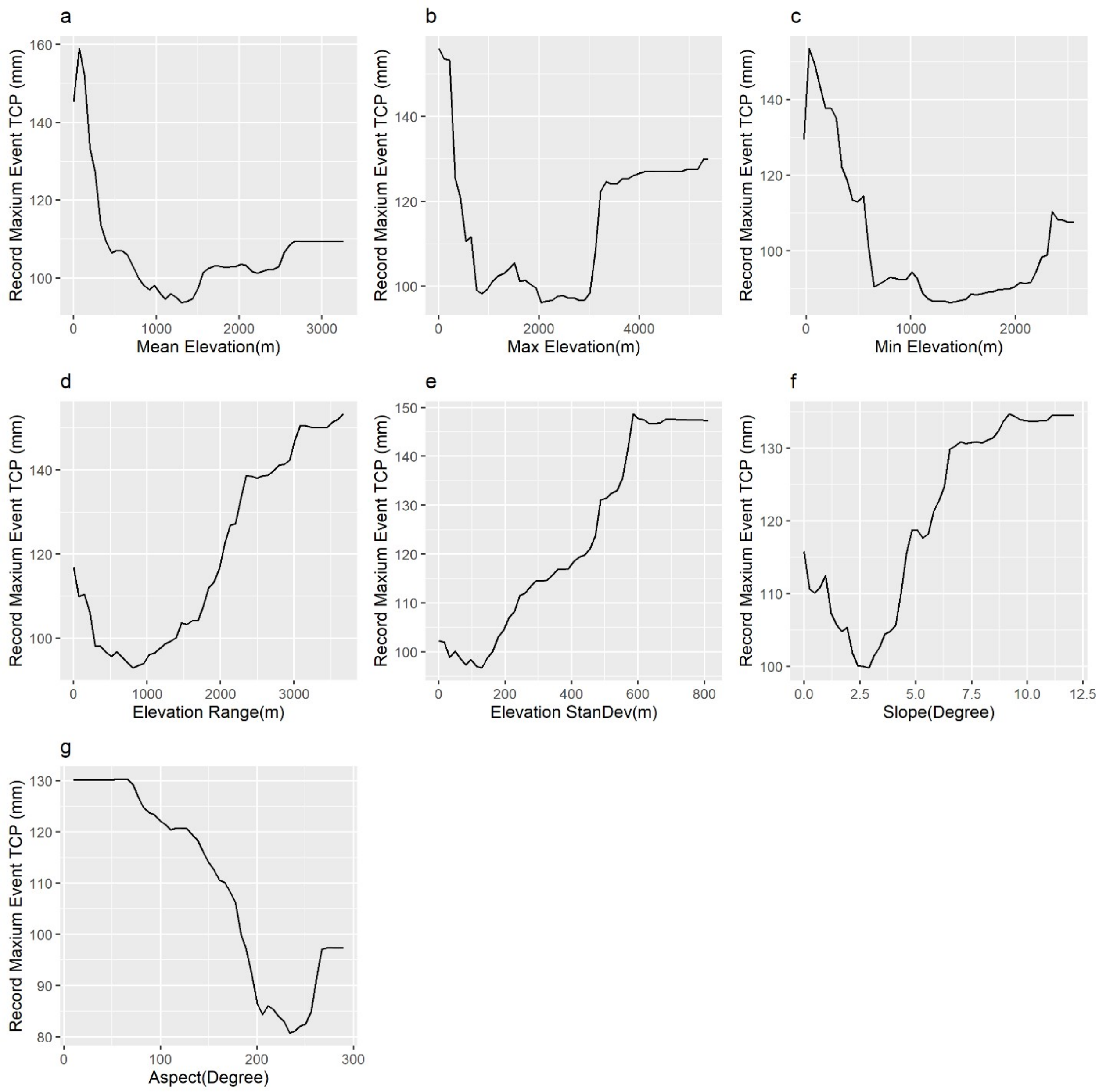

Figure 7. Partial Importance Plot for variables in the topographic RF model for the Maximum Event TCP

Lower Mean, Max, and Min elevation generally correspond to higher TCP sensitivity and the sensitivity decreases with elevation increases in smaller ranges. TCP sensitivities start to increase at higher elevations and then keep stable. For example, there are sudden rises of TCP sensitivity at ~1300 meters and 2400 meters for the mean elevation (Figure 7a) and at 2800 m for the maximum elevation (Figure 7b). The MaxETCP has similar TCP sensitivity responses to the elevation Range and Standard Deviation (Figure 7d and e) with those in the AMTCP Total Model. After a small dip in the lower value regions, the TCP sensitivity starts to rise monotonously from a ~ 1000 meters Range and a 170 meters Standard Deviation. The "U" shape of the TCP sensitivity curve for the Slope (Figure 7f) is also showing a similar pattern with the Total model of ANTCP (Figure 5i). However, steeper slope ends are observing higher TCP sensitivity than the shallower slopes. And higher TCP sensitivity at steeper Slope appears in the partial dependence plots for most of the other Total and Topo TCP models, except the Total model for the ANTCP (Figure 5i). Based on both the importance of the Slope variable in those models and these recurring patterns, we conclude that steeper Slopes generally lead to higher chances of modification of TCP in Mexico. The partial importance of the Aspect (Figure 7g) follows the same pattern with the Total model but with more distinct drops of TCP sensitivity when the Slope starts to turn to the lee direction to the Gulf of Mexico (Aspect > 180°). The coupled variable TCP partial dependence plots (Figure 8) are showing even more clear-cut patterns than those for the total models. Figure 8a has the highest TCP sensitivity for that the Aspect is between 90° to 180° and the Range is greater than 2000 m. The high TCP sensitivity zone for the high Range appears again in Figure 8b, together with the Max elevation is greater than 2000 m. Except for a high zone under ~ 300 m mean elevation, the TCP sensitivity generally increases with higher elevation standard deviation (Figure 8c). The highest TCP sensitivity is reached when the standard deviation is greater than 700 m and the mean elevation is greater than 1500 m.

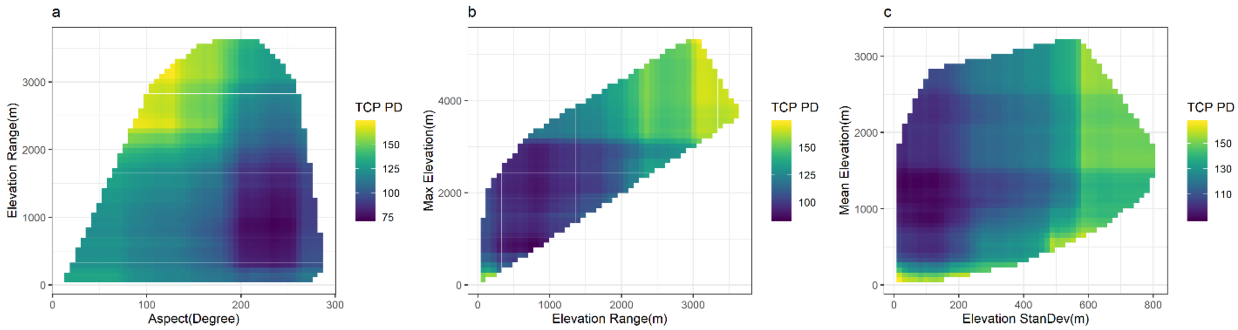

Figure 8. Selected Partial Dependence (PD) Plots for coupled variables in the topographic RF model for the Maximum Event TCP.

We use the partial dependence plots for the Total model of ANTCP and the Topographic model of MaxETCP as two examples. Partial dependence plots for all other models are displayed from supplement 3 to 10. Generally, the sensitivities of TCP variables behave in a consistent way to the changes of independent variables across different models. That gives us confidence that the RF can accurately capture the complex relationships between environmental variables (particularly topographic ones) and TCP characteristics based on the long climatology. They provide us a quantitative evaluation of which variable is most important to variations of the TCP and how the TCP is sensitive to different ranges of the topographic variables. That is very helpful for us to identify thresholds of changes when we study details about how topography influences the TCP from other methods in the future.

d. Extreme Cases

The final section of the data analysis is focused on the case study of three storms that produced the most intense TCP in the 99 years of Mexico climatology. They are Hurricane Alex in 2010, Hurricane Igrid in 2013 and Major Hurricane Beulah in 1967. Alex and Igrid are originated from tropical disturbances from the Gulf of Mexico or the Caribbean Sea and experience rapid intensification in a short translation distance before they made the landfall. Beulah is originated from the Atlantic Ocean and gathered a large amount of energy through its long translation distance before it became the major hurricane that made landfall first in Texas. We can observe large areas of extreme TCP for Hurricane Beulah for both Southern Texas and northeastern Mexico (Here we display all TCP without country border in the maps but calculate the statistics only for grids in Mexico). All three storms have produced > 400 mm precipitation at some locations (Figure 9 a, c, and e) and those extreme precipitations caused massive flooding and landslides with large losses of lives and infrastructures.

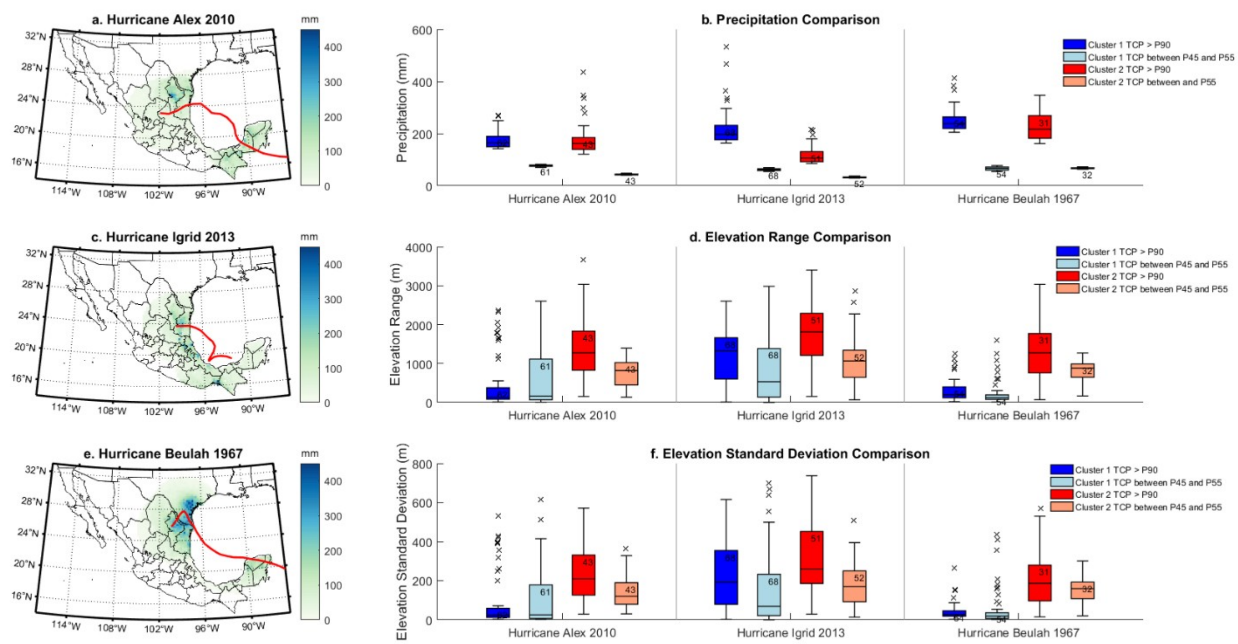

Figure 9. The total precipitation for the three most intense TCP events for Mexico and comparison of topographic variables between locations with extreme TCP (>P_{90}) and median TCP (between P_{45} and P_{55})

Here we process the topography comparison for the quantile event TCP again for each storm. We choose those greater than 90 percentile (P_{90}) TCP as the extreme values and those between 45 (P_{45}) and 55 (P_{55}) percentile TCP as the median values because the sample size of grids for a single storm is much smaller than the whole dataset. Figure 9b, d, and f compare the precipitation, elevation Range, and Standard Deviation for grid locations grouped by quantile TCPs for Cluster 1 and 2 separately. Table 6 and Supplement 11 are statistics of their median with the Mann-Whitney U-test. The P_{90} TCPs are much larger than the median TCP in most cases with at least 150 mm difference (Figure 9b and Table 6). Those big differences in precipitation are very closely related to differences in topographic complexity. In Figure 9d, most extreme TCP associated elevation Range samples have larger medians than the samples associated with median precipitation for all three storms. Particularly, those differences are even larger for the comparison for Cluster 2 (red and orange boxes). The same information is also demonstrated in Table 6, where most of the Mann-Whitney U-test for the sample median comparisons are statistically significant (with "+" sign in table 6). One exception is in the comparison for Cluster 1 in Hurricane Alex. Hurricane Alex has a large area of extreme precipitation over the Yucatan Peninsular for its first landfall and Yucatan is mostly covered by flatter terrains. The comparison for the elevation Standard Deviation is demonstrating the similar patterns (Figure 9f) as the elevation range. Four out of six comparisons show that the extreme TCP associated Elevation Standard Deviations is significantly larger than those with the median TCP (Supplement 11).

The extreme case study shows us that even there are lots of uncertainty and variability in the individual storm, the most extreme storms still demonstrate a very strong topographic enhancing effect for the TCP. This effect is existing in both coastal areas (Cluster 1 grids) the inland areas that are close to the coast (Cluster 2 grids). Cluster 2 grids have more distinctive patterns for this topographic enhancing effect. Directly from the precipitation maps in Figure 9, we can observe that in all three storms, clusters of maxima of precipitation are located in some inland areas in addition to locations on the coast where storms just made landfall.

4 Discussions and Conclusions.

The interactions between TCs and the topographic features over the land is a challenging topic because they are affected by so many factors together, and it becomes even more complex if we are focused on precipitation generated by TCs. There are many variations in storms, include their energy and moisture budget, storm size, tracks, etc. All those storm elements will have impacts on the locations and intensities of TCP. When TCs are translating from the ocean to the land, the boundary layer condition will significantly be changed and influence the behavior of TCs. The increase of surface roughness is believed to be an important contributor to the enhanced advection in the TC system, which introduces more TCP (Arndt et al., 2009; Kimball, 2008; Tuleya, 1994; Zhang et al., 2018). The complex terrain is one of the most important surface roughness factor that contributes to enhanced precipitation from the clouds, including those from the TCs (Houze, 2010, 2012).

Mexico is a country prone to strikes of TCs and its complex terrain has already triggered intense precipitation events that led to massive flooding events. However, how the terrains are interacting with the TC systems and influence their precipitation patterns has not been studied thoroughly, particularly for the windward side of the Sierra Madre Oriental. Our analysis is based on the longest available record of gauge observed TCP for Mexico since 1920 and we use both traditional and modern statistical data-mining techniques to discover relationships between the TCP and the topographic features. Our results demonstrate that locations (latitudes and distance to the coast) are the most dominant controller of the TCP variations in Mexico. The direct correlation between topography features and TCP variables does not reveal much information about the orographic enhancement because there is also a strong relationship between topography variables and their locations. Negative correlations are dominating between TCP and topography variables for the whole dataset. The spatial comparison between topographic variables and TCP shows that there are isolated and clustered inland locations with enhanced TCP statistics. A lot of those locations are also demonstrating a high amount of elevation variabilities.

To quantify the relationship between TCP and topography, we divided the whole grids set into six subgroups (clusters) using the K-Means clustering based on each grid's distance to the nearest coastal line. The correlation analysis demonstrates a significant change compared with the result of the whole data. Elevation variance variables (Range, Standard Deviation, and Slope) are showing statistically significant positive relationships with TCP variables, while other elevation variables (Mean, Max, and Min) are still demonstrating negative relationships. Cluster 2 (inland grids that nearest to the coast) is showing stronger average positive correlations between elevation variance variables and the TCPs than the Cluster 1(coast). If we look at the most extreme cases of TCP, they tend to happen at locations with a higher amount of elevation variance. The most extreme TCP locations have a much higher elevation Range and Standard Deviation than the median and trivial TCP locations. The comparisons for the daily TCP are all statistically significant. On the event scale, only the Cluster 2 comparisons are statistically significant. This result agrees with many previous theoretical and modeling studies based on TC cases. R. B. Smith et al. (2009) found that the Hurricane Dean had the orographic precipitation enhancement within 92 km of Dominica, they are more likely from the seeder–feeder accretion mechanism in a nearly stationary spiral rainband. The uplifting phenomenon is more common when the TCs meet larger mountain ranges. In a simulation study for an Australia TC (Ramsay

& Leslie, 2008), the TCP reduced immediately after landfall but was enhanced when the storm met the steep coastal orography and the wind field has been substantially modified. The mountain lifting of TCs was extensively studied for the CMR of Taiwan Island. TCs are modified in their 3-D flows, precipitation, or even tracks while they are passing the CMR (Chang et al., 2013; Lin et al., 2002; Wu et al., 2002; Yu & Cheng, 2008). The deflection of storm tracks by mountains has also been investigated in Taiwan island (Lin et al., 2005) and the Sierra Madre Occidental of western Mexico (Farfán & Zehnder, 2001; Zehnder, 1993). The result from our analysis shows that the complex topography has a strong enhancing effect to the TCP in this area. Based on the size of the Sierra Madre Oriental and the statistical analysis, we believe this enhancement is more likely to be the cloud uplifting effect. But it will need more observations and numerical simulations to prove it.

The RF model has been proved to be an effective tool to explore the relationships between environment variables (both location and topography) and the TCP. The RF model explains more variances than the traditional statistical models. Multivariate regression models can obtain an explained variance between 31% to 75% of the annual precipitation in different mountainous areas around the world (Basist et al., 1994). Our RF models are showing 47% to 96% variances of different TCP characteristics based on the fact that the TCP has more uncertainties than the annual mean precipitation. The correlation analysis or multiple regression models can only show influence from one or several environment variables to the TCP because of the nature of the statistical methods and the distribution of the variables. The RF model excels in including different explanatory variables with different kinds of distribution and revealing their relationships with the response variable collectively. Our result demonstrates that the location variables (particular the distance to the coast) are the most important factor in influencing the TCP in all total models and the aspect of the Slope is the most important factor in all topography models. The mountain ranges that are in the windward of the Gulf are demonstrating higher sensitivity in the amount of TCP and the probability in extreme TCP, particularly between 120° to 180°. The TCP sensitivity has non-linear responses to some topographic variables. Some TCP variables are demonstrating a dipole pattern in their sensitivity responses to several elevation variables. The first high sensitivities of TCP appear at regions with very low elevation and shallow Slopes due to the high variability in the TCP dynamics right after landfall. Another high TCP sensitivity zone is also pronounced at regions with higher elevation (max elevation > 3000 m) and more complex terrains (elevation range > 2000 m, slope > 5°, and Elevation Standard Deviation > 500 m), which is very likely to be the topographic enhancing effect of TCP. The RF model can capture these two separate processes with big impacts on the TCP very well.

The interaction between individual TC and topography is complicated by the storm's track, landfall positions, storm size, intensity, amount of moisture, and influences from other weather systems over land. We have selected three storms that have produced the largest amount of total TCP between 1920 and 2018. All of them made landfall near the northeastern corner of Mexico with some degree of deflections in their tracks. Although some previous research mentioned that storm tracks can be deflected by the orography (Chang et al., 2013; Farfán & Zehnder, 2001; Lin et al., 2002; Wu et al., 2002), we need more numeric experiments and observations to fully understand the mechanisms for storms in our study. The deflection does extend the time that a storm staying at one location and increases the possibility of orographic enhancement of precipitation in three storms we have chosen. Similar to the maps for the TCP statistics of the whole dataset, the maps for the TCP of the maximum cases also show maximum

TCPs over mountainous areas with complex topography. Those most extreme TCP events have a median of ~ 200 mm with the possibility of exceeding 400 mm occasionally. That intensity of precipitation could trigger severe flash flooding and landslide in those areas (Salinas-Jasso et al., 2020). Our result shows that the locations with the most intense TCP in those three storms have a statistically significant larger elevation Range and Standard Deviation than those with median TCPs. The topographic enhancing effect of TCP is very strong at the storm level, shown by the three most extreme TCP cases. This effect is more pronounced in Cluster 2 grids, which have higher mean elevation and more complex terrains.

Our analysis is based on long term gauge observed precipitation at the daily interval and 1km resolution DEM data. We have clearly shown very strong statistical relationships between TCP variables and topographic features, which indicates the enhancing effect of the Sierra Madre Oriental to the TCP from the TCs on the Gulf side. The same effect has been shown by the whole dataset as well as the most extreme TCP cases. The RF models can provide certain ranges of topographic variables (elevation Range, Slope, and Aspect) that have particularly high sensitivity of TCP. The study is limited by the dimension of the observation and the temporal resolution of the data. The orographic effects on rainfalls are closely related to the directions of 3-D flows, as well as the energy, temperature, and moisture distribution at different altitudes. Rain gauges can only provide precipitation observation at the surface level for a long period. We need more 3-D observations to understand the more detailed precipitation mechanisms for each storm in the future. The finest tempo-resolution for our data is daily, which might not be able to capture some rapid precipitation processes at the sub-daily or even finer time scales. The spatial distribution of rain gauges may occasionally be not enough to capture the detailed spatial distribution of TCP, which leads to under-sampling issues while we are processing the IDW spatial interpolation. In the future, we can refer to TRMM Multi-satellite Precipitation Analysis (TMPA) or the newest Integrated Multi-Satellite Retrievals (IMERG) for Global Precipitation Measurement (GPM) for much detailed rain ratios in most recent TCs. We also plan to set up numerical models (both regional and global) to test the statistical relationships we have found from the observations.

Acknowledgments

This research is supported by the NSF Grant #1619681: The Michigan Louis Stokes Alliance for Minority Participation (MI-LSAMP)

Gauge observations are derived from the Daily Global Historical Climatology Network (GHCN-D) (https://www.ncdc.noaa.gov/ghcnd-data-access) and obtained from the National Weather Service of Mexico by requiring. Tropical cyclone tracks are obtained from International Best Track Archive for Climate Stewardship (IBTrACS) (https://www.ncdc.noaa.gov/ibtracs/). The DEM data is obtained from the USGS EROS Archive - Digital Elevation - Global 30 Arc-Second Elevation (GTOPO30) (https://www.usgs.gov/centers/eros/science/usgs-eros-archive-digital-elevation-global-30-arc-second-elevation-gtopo30?qt-science_center_objects=0#qt-science_center_objects)

References

Agustín Breña-Naranjo, J., Pedrozo-Acuña, A., Pozos-Estrada, O., Jiménez-López, S. A., & López-López, M. R. (2015). The contribution of tropical cyclones to rainfall in Mexico. *Physics and Chemistry of the Earth, Parts A/B/C, 83-84*, 111-122. doi:https://doi.org/10.1016/j.pce.2015.05.011

Arndt, D. S., Basara, J. B., McPherson, R. A., Illston, B. G., McManus, G. D., & Demko, D. B. (2009). Observations of the Overland Reintensification of Tropical Storm Erin (2007). *Bulletin of the American Meteorological Society, 90*(8), 1079-1094. doi:10.1175/2009bams2644.1

Basist, A., Bell, G. D., & Meentemeyer, V. (1994). Statistical Relationships between Topography and Precipitation Patterns. *Journal of Climate, 7*(9), 1305-1315. doi:10.1175/1520-0442(1994)007<1305:srbtap>2.0.co;2

Bender, M. A., Tuleya, R. E., & Kurihara, Y. (1985). A Numerical Study of the Effect of a Mountain Range on a Landfalling Tropical Cyclone. *Monthly Weather Review, 113*(4), 567-583. doi:10.1175/1520-0493(1985)113<0567:ansote>2.0.co;2

Bender, M. A., Tuleya, R. E., & Kurihara, Y. (1987). A Numerical Study of the Effect of Island Terrain on Tropical Cyclones. *Monthly Weather Review, 115*(1), 130-155. doi:10.1175/1520-0493(1987)115<0130:ansote>2.0.co;2

Bergeron, T. (1968). Studies of the orogenic effect on the areal fine structure of rainfall distribution. In (Vol. Rep. 6, pp. 42). Uppsala University Meteorological Institute

Best, D. J., & Roberts, D. E. (1975). Algorithm AS 89: The Upper Tail Probabilities of Spearman's Rho. *Journal of the Royal Statistical Society. Series C (Applied Statistics), 24*(3), 377-379. doi:10.2307/2347111

Breiman, L. (2001). Random forests. *Machine Learning, 45*(1), 5-32. doi:10.1023/a:1010933404324

Breiman, L., Friedman, J., Stone, C. J., & Olshen, R. A. (1984). *Classification and Regression Trees*. U.S.A: Taylor & Francis.

Burrough, P. A., McDonnell, R. A., & Lloyd, C. D. (2015). *Principles of geographical information systems*. Oxford: Oxford University Press.

Chan, J. C. L. (2005). THE PHYSICS OF TROPICAL CYCLONE MOTION. *Annual Review of Fluid Mechanics, 37*(1), 99-128. doi:10.1146/annurev.fluid.37.061903.175702

Chang, C. P., Yang, Y. T., & Kuo, H. C. (2013). Large Increasing Trend of Tropical Cyclone Rainfall in Taiwan and the Roles of Terrain. *Journal of Climate, 26*(12), 4138-4147. doi:10.1175/jcli-d-12-00463.1

Emanuel, K. (2017). Assessing the present and future probability of Hurricane Harvey's rainfall. *Proceedings of the National Academy of Sciences, 114*(48), 12681-12684. doi:10.1073/pnas.1716222114

Farfán, L. M., & Cortez, M. (2005). An Observational and Modeling Analysis of the Landfall of Hurricane Marty (2003) in Baja California, Mexico. *Monthly Weather Review, 133*(7), 2069-2090. doi:10.1175/mwr2966.1

Farfán, L. M., & Zehnder, J. A. (2001). An Analysis of the Landfall of Hurricane Nora (1997). *Monthly Weather Review, 129*(8), 2073-2088. doi:10.1175/1520-0493(2001)129<2073:Aaotlo>2.0.Co;2

Franco-Díaz, A., Klingaman, N. P., Vidale, P. L., Guo, L., & Demory, M.-E. (2019). The contribution of tropical cyclones to the atmospheric branch of Middle America's hydrological cycle using observed and reanalysis tracks. *Climate Dynamics, 53*(9-10), 6145-6158. doi:10.1007/s00382-019-04920-z

Greenwell, B. M. (2017). pdp: An R Package for Constructing Partial Dependence Plots. *The R Journal, 9*(1), 421–436.

Houze, R. A. (2010). Clouds in Tropical Cyclones. *Monthly Weather Review, 138*(2), 293-344. doi:10.1175/2009mwr2989.1

Houze, R. A. (2012). Orographic effects on precipitating clouds. *Reviews of Geophysics, 50*(1). doi:10.1029/2011rg000365

Huang, C.-Y., Chou, C.-W., Chen, S.-H., & Xie, J.-H. (2020). Topographic Rainfall of Tropical Cyclones past a Mountain Range as Categorized by Idealized Simulations. *Weather and Forecasting, 35*(1), 25-49. doi:10.1175/waf-d-19-0120.1

Kepert, J. (2001). The Dynamics of Boundary Layer Jets within the Tropical Cyclone Core. Part I: Linear Theory. *Journal of the Atmospheric Sciences, 58*(17), 2469-2484. doi:10.1175/1520-0469(2001)058<2469:Tdoblj>2.0.Co;2

Kimball, S. K. (2008). Structure and Evolution of Rainfall in Numerically Simulated Landfalling Hurricanes. *136*(10), 3822-3847. doi:10.1175/2008mwr2304.1

Knutson, T., Camargo, S. J., Chan, J. C. L., Emanuel, K., Ho, C.-H., Kossin, J., . . . Wu, L. (2019). Tropical Cyclones and Climate Change Assessment: Part I: Detection and Attribution. *Bulletin of the American Meteorological Society, 100*(10), 1987-2007. doi:10.1175/bams-d-18-0189.1

Langousis, A., & Veneziano, D. (2009). Theoretical model of rainfall in tropical cyclones for the assessment of long-term risk. *Journal of Geophysical Research, 114*(D2). doi:10.1029/2008jd010080

Li, Y., Huang, W., & Zhao, J. (2007). Roles of mesoscale terrain and latent heat release in typhoon precipitation: A numerical case study. *Advances in Atmospheric Sciences, 24*(1), 35-43. doi:10.1007/s00376-007-0035-8

Lin, Y.-L., Chen, S.-Y., Hill, C. M., & Huang, C.-Y. (2005). Control Parameters for the Influence of a Mesoscale Mountain Range on Cyclone Track Continuity and Deflection. *Journal of the Atmospheric Sciences, 62*(6), 1849-1866. doi:10.1175/jas3439.1

Lin, Y.-L., Ensley, D. B., Chiao, S., & Huang, C.-Y. (2002). Orographic Influences on Rainfall and Track Deflection Associated with the Passage of a Tropical Cyclone. *Monthly Weather Review, 130*(12), 2929-2950. doi:10.1175/1520-0493(2002)130<2929:Oiorat>2.0.Co;2

Lu, P., Lin, N., Emanuel, K., Chavas, D., & Smith, J. (2018). Assessing Hurricane Rainfall Mechanisms Using a Physics-Based Model: Hurricanes Isabel (2003) and Irene (2011). *Journal of the Atmospheric Sciences, 75*(7), 2337-2358. doi:10.1175/jas-d-17-0264.1

Mann, H. B., & Whitney, D. R. (1947). On a Test of Whether one of Two Random Variables is Stochastically Larger than the Other. *Ann. Math. Statist., 18*(1), 50-60. doi:10.1214/aoms/1177730491

Mascaro, G., Vivoni, E. R., Gochis, D. J., Watts, C. J., & Rodriguez, J. C. (2014). Temporal Downscaling and Statistical Analysis of Rainfall across a Topographic Transect in Northwest Mexico. *Journal of Applied Meteorology and Climatology, 53*(4), 910-927. doi:10.1175/jamc-d-13-0330.1

Pan, C. J., Lai, H. C., Yang, S. S., Reddy, K. K., & Chang, S. C. (2008). Wind profiler radar investigation on typhoon-orography interaction. *35*(24). doi:10.1029/2008gl036368

Pineda-Martinez, L. F., & Carbajal, N. (2009). Mesoscale numerical modeling of meteorological events in a strong topographic gradient in the northeastern part of Mexico. *Climate Dynamics, 33*(2-3), 297-312. doi:10.1007/s00382-009-0549-0

Ramsay, H. A., & Leslie, L. M. (2008). The Effects of Complex Terrain on Severe Landfalling Tropical Cyclone Larry (2006) over Northeast Australia. *Monthly Weather Review, 136*(11), 4334-4354. doi:10.1175/2008mwr2429.1

Risser, M. D., & Wehner, M. F. (2017). Attributable Human-Induced Changes in the Likelihood and Magnitude of the Observed Extreme Precipitation during Hurricane Harvey. *Geophysical Research Letters, 44*(24), 12,457-412,464. doi:10.1002/2017gl075888

Salinas-Jasso, J. A., Velasco-Tapia, F., Navarro De León, I., Salinas-Jasso, R. A., & Alva-Niño, E. (2020). Estimation of rainfall thresholds for shallow landslides in the Sierra Madre Oriental, northeastern Mexico. *Journal of Mountain Science, 17*(7), 1565-1580. doi:10.1007/s11629-020-6050-2

Shapiro, L. J. (1983). The Asymmetric Boundary layer Flow Under a Translating Hurricane. *Journal of the Atmospheric Sciences, 40*(8), 1984-1998. doi:10.1175/1520-0469(1983)040<1984:Tablfu>2.0.Co;2

Smith, R. B. (1979). The Influence of Mountains on the Atmosphere. In B. Saltzman (Ed.), *Advances in Geophysics* (Vol. 21, pp. 87-230): Elsevier.

Smith, R. B., Schafer, P., Kirshbaum, D., & Regina, E. (2009). Orographic Enhancement of Precipitation inside Hurricane Dean. *Journal of Hydrometeorology, 10*(3), 820-831. doi:10.1175/2008jhm1057.1

Trenberth, K. E., Cheng, L., Jacobs, P., Zhang, Y., & Fasullo, J. (2018). Hurricane Harvey Links to Ocean Heat Content and Climate Change Adaptation. *Earth's Future, 6*(5), 730-744. doi:10.1029/2018ef000825

Tuleya, R. E. (1994). Tropical Storm Development and Decay: Sensitivity to Surface Boundary Conditions. *Monthly Weather Review, 122*(2), 291-304. doi:10.1175/1520-0493(1994)122<0291:tsdads>2.0.co;2

Vivoni, E. R., Gutiérrez-Jurado, H. A., Aragón, C. A., Méndez-Barroso, L. A., Rinehart, A. J., Wyckoff, R. L., . . . Jackson, T. J. (2007). Variation of Hydrometeorological Conditions along a Topographic Transect in Northwestern Mexico during the North American Monsoon. *Journal of Climate, 20*(9), 1792-1809. doi:10.1175/jcli4094.1

Wu, C. C., Yen, T. H., Kuo, Y. H., & Wang, W. (2002). Rainfall simulation associated with typhoon herb (1996) near Taiwan. Part I: The topographic effect. *Weather and Forecasting, 17*(5), 1001-1015. doi:10.1175/1520-0434(2003)017<1001:Rsawth>2.0.Co;2

Yu, C.-K., & Cheng, L.-W. (2008). Radar Observations of Intense Orographic Precipitation Associated with Typhoon Xangsane (2000). *Monthly Weather Review, 136*(2), 497-521. doi:10.1175/2007mwr2129.1

Zehnder, J. A. (1993). The Influence of Large-Scale Topography on Barotropic Vortex Motion. *Journal of the Atmospheric Sciences, 50*(15), 2519-2532. doi:10.1175/1520-0469(1993)050<2519:Tiolst>2.0.Co;2

Zhang, W., Villarini, G., Vecchi, G. A., & Smith, J. A. (2018). Urbanization exacerbated the rainfall and flooding caused by hurricane Harvey in Houston. *Nature, 563*(7731), 384-388. doi:10.1038/s41586-018-0676-z

Zhu, L., & Quiring, S. M. (2017). An Extraction Method for Long-Term Tropical Cyclone Precipitation from Daily Rain Gauges. *Journal of Hydrometeorology, 18*(9), 2559-2576. doi:10.1175/jhm-d-16-0291.1